

## Electronic structure and lattice dynamics of $\text{Li}_x\text{CoO}_2$ single crystals

This content has been downloaded from IOPscience. Please scroll down to see the full text.

2015 New J. Phys. 17 103004

(<http://iopscience.iop.org/1367-2630/17/10/103004>)

View [the table of contents for this issue](#), or go to the [journal homepage](#) for more

Download details:

IP Address: 140.122.161.93

This content was downloaded on 01/10/2015 at 02:09

Please note that [terms and conditions apply](#).



## PAPER

Electronic structure and lattice dynamics of  $\text{Li}_x\text{CoO}_2$  single crystals

## OPEN ACCESS

RECEIVED  
1 June 2015REVISED  
6 September 2015ACCEPTED FOR PUBLICATION  
9 September 2015PUBLISHED  
30 September 2015Content from this work  
may be used under the  
terms of the [Creative  
Commons Attribution 3.0  
licence](#).Any further distribution of  
this work must maintain  
attribution to the  
author(s) and the title of  
the work, journal citation  
and DOI.H L Liu<sup>1,6</sup>, T Y Ou-Yang<sup>2,3</sup>, H H Tsai<sup>1</sup>, P A Lin<sup>4,5</sup>, H T Jeng<sup>4</sup>, G J Shu<sup>3</sup> and F C Chou<sup>3</sup><sup>1</sup> Department of Physics, National Taiwan Normal University, Taipei 11677, Taiwan<sup>2</sup> Department of Physics, National Taiwan University, Taipei 10617, Taiwan<sup>3</sup> Center for Condensed Matter Sciences, National Taiwan University, Taipei 10617, Taiwan<sup>4</sup> Department of Physics, National Tsing Hua University, Hsinchu 30013, Taiwan<sup>5</sup> Center for Measurement Standards, Industrial Technology Research Institute, Hsinchu 31040, Taiwan<sup>6</sup> Author to whom any correspondence should be addressed.E-mail: [hliu@ntnu.edu.tw](mailto:hliu@ntnu.edu.tw)**Keywords:** strongly correlated electron system, optical properties, Raman and optical spectroscopy**Abstract**

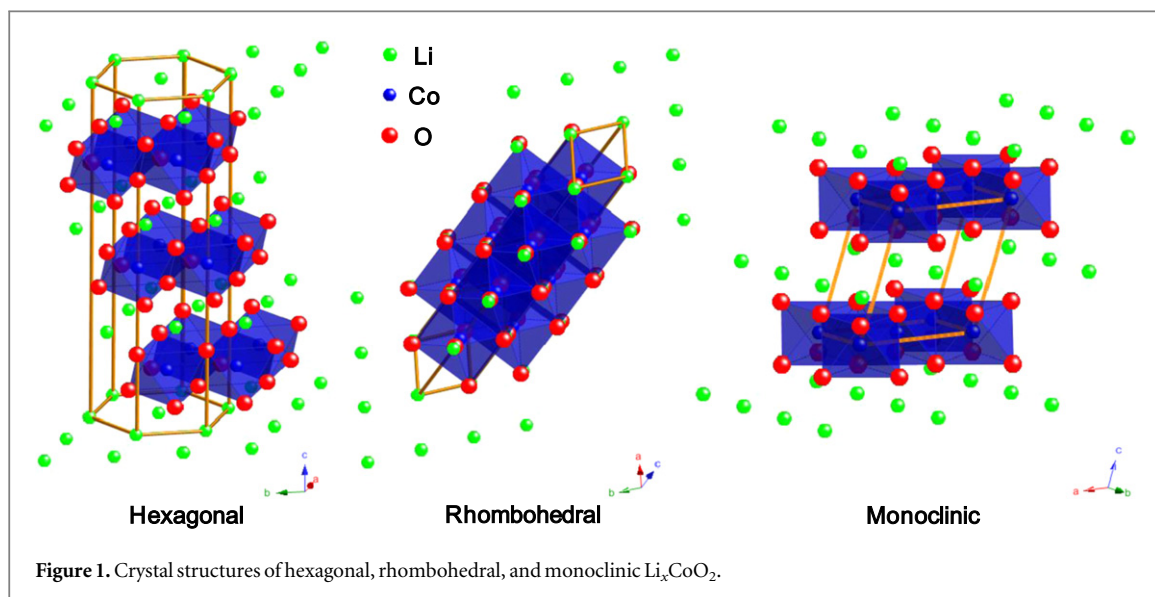
Spectroscopic ellipsometry and Raman scattering measurements of single-crystal  $\text{Li}_x\text{CoO}_2$  ( $x = 0.33, 0.43, 0.50, 0.53, 0.72$ , and  $0.87$ ) are reported. The room temperature optical absorption spectra for  $x$  values in the range of  $0.33$ – $0.72$  exhibit three bands near  $1.60, 3.35$ , and  $5.20$  eV. On the basis of first-principles calculations, the observed optical excitations were appropriately assigned. The charge-transfer absorption bands shift to higher energies in  $\text{Li}_{0.87}\text{CoO}_2$  because of symmetry-breaking-induced distortions of the hybridized Co-O orbitals with shifted oxygen  $2p$  states. Furthermore, two Raman-active phonon modes, which display  $E_g$  and  $A_{1g}$  symmetry, are sensitive to lithium doping. Upon cooling across  $200$  K, which is the antiferromagnetic phase transition temperature of  $\text{Li}_{0.50}\text{CoO}_2$ , large splitting of the  $E_g$  mode and a discontinuous change in the frequency of the  $A_{1g}$  mode were observed. These results highlight the importance of spin-phonon coupling in  $\text{Li}_{0.50}\text{CoO}_2$ .

**1. Introduction**

Layered lithium cobaltites ( $\text{Li}_x\text{CoO}_2$ ) have attracted considerable attention in recent years. The interest has been stimulated not only by their practical applications as rechargeable battery electrode materials and electrochromic displays [1, 2], but also by a need to understand the mechanism underlying their complex physical properties [3–9]. The fully lithiated compound with stoichiometry  $\text{LiCoO}_2$  has a hexagonal structure belonging to the  $R\bar{3}m$  space group. The building blocks are edges-sharing  $\text{CoO}_6$  octahedra; the edges are linked to form  $\text{CoO}_2$  sheets and they are separated by layers of lithium atoms, as shown in figure 1 [10]. During the oxidation of  $\text{Li}_x\text{CoO}_2$ , the crystal structure can be described by a rhombohedral group. A monoclinic phase appears in the compound of  $x = 0.50$  [7, 9, 10]. Furthermore, depending on the lithium content,  $\text{Li}_x\text{CoO}_2$  exhibits various interesting electronic, magnetic, and thermoelectric properties [3, 5–9].

$\text{LiCoO}_2$  is an insulator with a band gap of  $2.7$  eV [11, 12]. Its magnetic susceptibility is low and shows weak temperature dependence because of the nonmagnetic low-spin state of  $\text{Co}^{3+}$  ( $t_{2g}^6$ ) ions [6]. The delithiated compound  $\text{Li}_x\text{CoO}_2$  contains  $\text{Co}^{4+}$  ( $t_{2g}^5$ ) ions and shows hole doping in the  $t_{2g}$  orbitals.  $\text{Li}_x\text{CoO}_2$  with  $x \geq 0.94$  is semiconducting, whereas the highly Li-deficient phase ( $0.75 \geq x \geq 0.25$ ) exhibits a metallic character [7, 13, 14]. At  $x = 0.75$ , unusually high thermoelectric power and metallic conductivity appear simultaneously [8]. In the ranges of  $x \geq 0.94$  and  $0.75 \geq x \geq 0.50$ ,  $\text{Li}_x\text{CoO}_2$  shows Curie–Weiss behavior, whereas it becomes Pauli-paramagnetic for  $x \leq 0.40$  [3, 5–8]. Notably, for  $x = 0.50$  and  $0.67$ , a magnetic anomaly is observed near  $175$  K [6]. For  $x = 0.40$ , a susceptibility hump is detected at  $30$  K [6]. All these observations suggest that the physical properties of these materials are complex.

Despite intense research having been conducted on layered lithium cobaltites, their optical and phonon properties have remained relatively unexplored [11, 12, 15–18]. Moreover, previous studies on  $\text{Li}_x\text{CoO}_2$  were limited to powder samples. Recently, we employed the electrochemical deintercalation method for synthesizing  $\text{Li}_x\text{CoO}_2$  single crystals [9]. A- and chain-type antiferromagnetic orderings were observed for  $x = 0.87$  and  $0.50$



at approximately 10 and 200 K [9]. For compounds with  $x = 0.53, 0.50,$  and  $0.43$ , three phases with distinct physical properties were identified [9]. The peculiar magnetic anomaly observed near 175 K for powder samples could be associated with a minor phase preferentially formed on the surface or at grain boundaries [9].

In this study, we employed both spectroscopic ellipsometry and Raman scattering spectroscopy to elucidate the electronic and phononic excitations of  $\text{Li}_x\text{CoO}_2$ , and we compared our results with the predictions of first-principles calculations. Understanding the intrinsic mechanisms governing the optical and phonon properties of  $\text{Li}_x\text{CoO}_2$  is vital for device applications. Our overall objective was to identify the doping dependence of the crystal architecture, electronic structure, and lattice dynamics relationships of  $\text{Li}_x\text{CoO}_2$ .

## 2. Technical details

### 2.1. Experiment

A series of single-crystal  $\text{Li}_x\text{CoO}_2$  samples with  $x = 0.33, 0.43, 0.50, 0.53, 0.72,$  and  $0.87$  were prepared through electrochemical deintercalation of pristine  $\text{Li}_{0.87}\text{CoO}_2$ . The details of sample preparation were reported elsewhere [9]. The crystals were thin platelets with dimensions of approximately  $2 \times 2 \times 0.5 \text{ mm}^3$ . Crystals of the same batch were characterized using synchrotron x-ray powder diffraction, dc resistivity, and magnetization measurements [9].

Spectroscopic ellipsometric measurements were performed for multiple angles of incidence between  $60^\circ$  and  $75^\circ$  by using a Woollam M-2000U ellipsometer over the spectral range 0.73–6.42 eV. The reproducibility of the spectra was confirmed at different regions on the sample surfaces by using a combination of focusing optics and spectroscopic ellipsometry for spot ( $100 \times 100 \mu\text{m}^2$ ) measurements.

Micro-Raman scattering experiments were performed in a backscattering geometry by using a diode-pumped solid-state laser with an excitation wavelength of 532 nm. The linearly polarized light was focused on a  $3 \mu\text{m}$  diameter spot on a sample surface, and the scattered light was collected and dispersed using a SENTERRA spectrometer equipped with a 1024 pixel wide charge-coupled detector. The polarizations of incident and scattered light were chosen so that they are parallel (parallel) or perpendicular (cross) to each other. The spectral resolution achieved using these instruments is typically less than  $1 \text{ cm}^{-1}$ . To avoid heating effects, the laser power was set to less than 0.2 mW. The sample was placed in a continuous-flow helium cryostat, which enabled measurements in the temperature range of 10–300 K.

### 2.2. Theoretical methods

We performed the first-principles calculations of electronic structure by using the full-potential projected-augmented-wave method as implemented in the VASP package within the generalized-gradient approximation (GGA) plus Hubbard  $U$  (GGA +  $U$ ) scheme [19–22]. The material  $\text{Li}_x\text{CoO}_2$  was simulated in the supercell approach under structure optimizations based on the experimental lattice structure [6]. The calculations were performed over 100  $k$ -points in the irreducible Brillouin zones with a cutoff energy of 400 eV. On-site Coulomb energy  $U = 4 \text{ eV}$  and exchange parameter  $J = 1 \text{ eV}$  were used for cobalt to explore the correlation effects in  $3d$  orbitals.

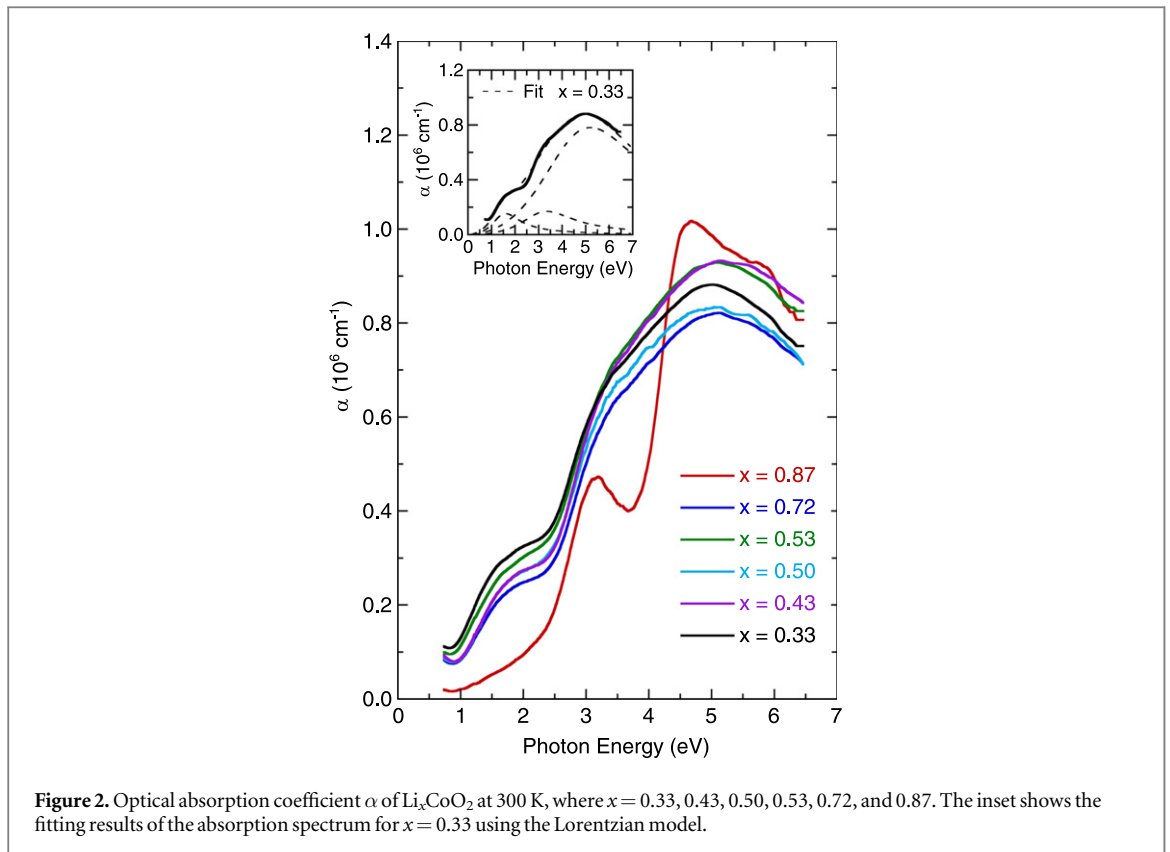


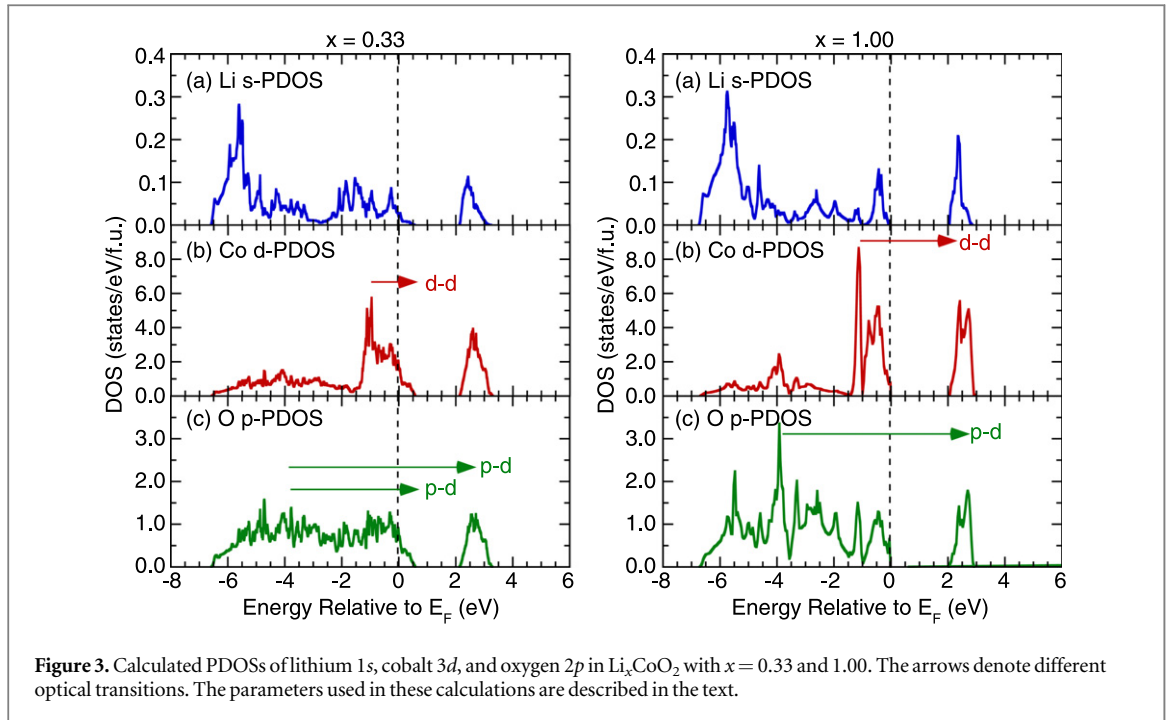
**Figure 2.** Optical absorption coefficient  $\alpha$  of  $\text{Li}_x\text{CoO}_2$  at 300 K, where  $x = 0.33, 0.43, 0.50, 0.53, 0.72,$  and  $0.87$ . The inset shows the fitting results of the absorption spectrum for  $x = 0.33$  using the Lorentzian model.

### 3. Results and discussion

#### 3.1. Electronic excitations

Figure 2 shows the room temperature optical absorption spectra of  $\text{Li}_x\text{CoO}_2$  obtained through spectroscopic ellipsometry analysis. These absorption spectra can be modeled reasonably well by using Lorentzian oscillators. For  $x = 0.33$ – $0.72$ , low-energy absorption shows a finite value. With an increase in the photon energies, the absorption gradually increases, manifests two bands near 1.60 and 3.35 eV, reaches a maximum value at approximately 5.20 eV, and then levels off. The positions of the three absorption peaks vary only slightly among the different lithium doping levels. By contrast, the low-energy absorption for  $x = 0.87$  is low, and the first low-energy peak near 1.60 eV completely disappears. The three absorption bands are observed at approximately 3.08, 4.55, and 5.76 eV, reflecting changes in the electronic structure of the compound.

To assign the observed absorption peaks of  $\text{Li}_x\text{CoO}_2$ , we calculated the partial densities of states (PDOSs) of lithium 1s, cobalt 3d, and oxygen 2p electrons for compounds with  $x = 0.33$  and 1.00 (figure 3). Three crucial features can be observed in figure 3. First, the magnitude of PDOS of lithium 1s is considerably smaller than that of other atoms, and therefore, the PDOS has no influence on the absorption bands. Second, the PDOS for  $x = 0.33$  exhibits nonzero electron density at the Fermi level, thereby reflecting metallic behavior. By contrast, the PDOS for  $x = 1.00$  evidences insulating behavior with a band gap of 2.0 eV. Third, both the highest occupied and lowest unoccupied levels mainly show a cobalt 3d character, while oxygen 2p orbitals contribute to a much smaller extent. On the basis of these theoretical calculation results, we assigned the observed excitation near 1.60 eV to the on-site *d-d* transition between the occupied cobalt *d* states right below  $E_F$  and the unoccupied *d* states. Its energy scale is comparable to that of the band calculated for  $\text{HoCoO}_3$  ( $\sim 2.04$  eV) and  $\text{LaCoO}_3$  ( $\sim 1.93$  eV) [23]. In principle, optical excitations between *d* orbitals are forbidden because of the selection rule for electric dipole transitions. However, strong hybridization between oxygen 2p and cobalt 3d orbitals leads to the breaking of local symmetry, thereby enabling these transitions [24]. The absorption peaks near 3.35 and 5.20 eV were assigned to charge-transfer transitions from the occupied hybridized oxygen 2p with cobalt 3d states to the unoccupied cobalt 3d states [25, 26]. Our results also show great similarity with the local density approximation calculations of  $\text{Na}_x\text{CoO}_2$  [27]. The observed 1.6 eV absorption peak in  $\text{Na}_x\text{CoO}_2$  ( $x = 0.25, 0.50, 0.70,$  and  $0.75$ ) [28, 29] corresponded to the transition from the occupied cobalt 3d  $t_{2g}$  to the empty cobalt 3d  $e_g$  states [27]. The higher energy absorption band at 3.1 eV observed in  $\text{Na}_x\text{CoO}_2$  [28, 29] was assigned to the transitions from the fully occupied oxygen 2p states to the unoccupied cobalt 3d  $e_g$  states [27].

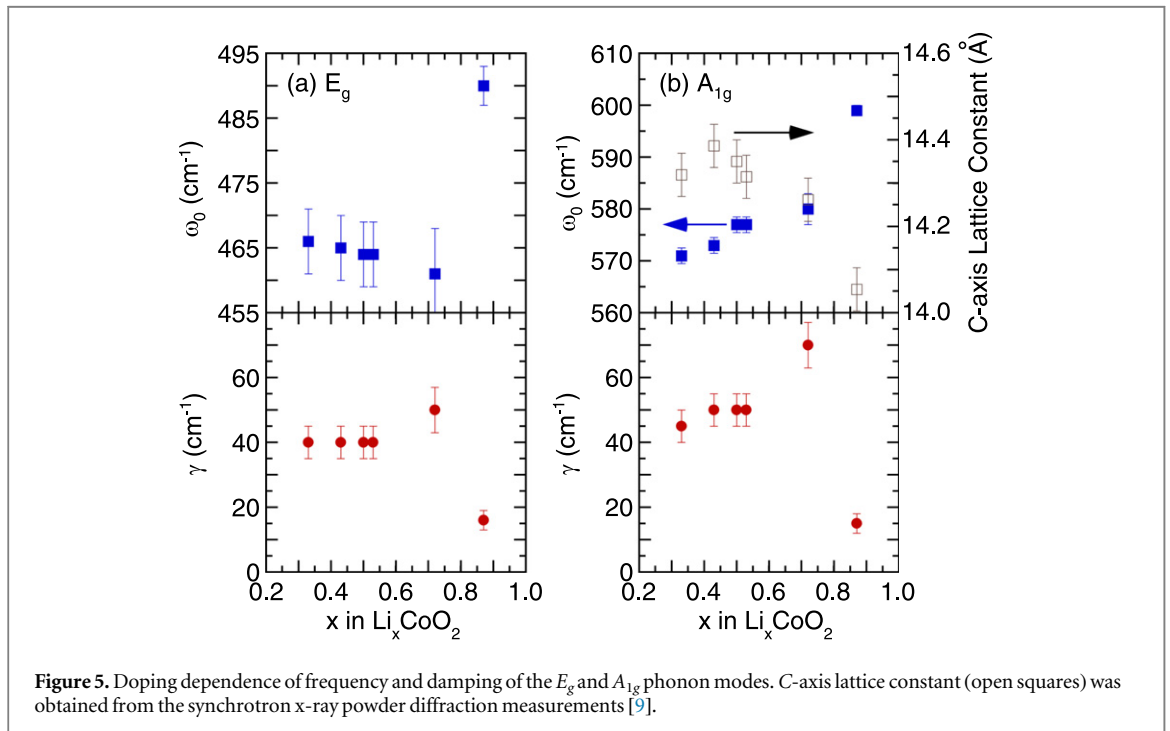
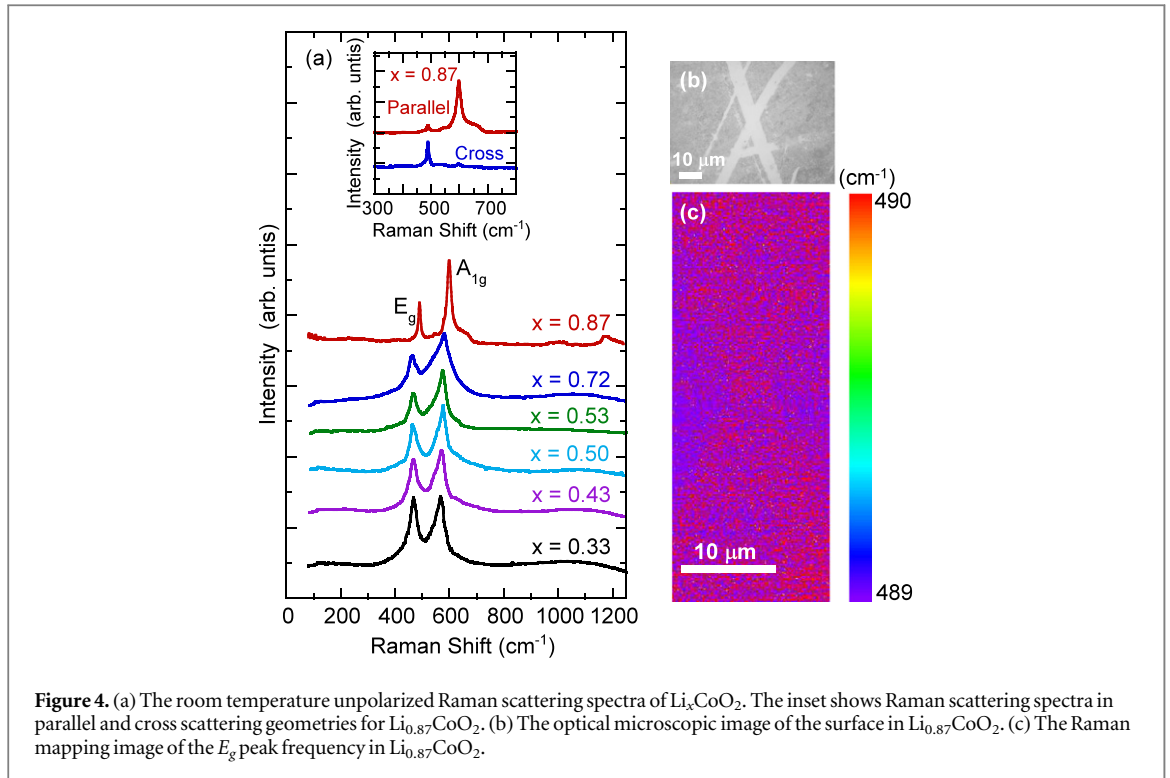


As mentioned, the absorption spectrum for  $x = 0.87$  is different from that for other lithium doping levels. We assigned the observed peak near 3.08 eV to the on-site  $d-d$  transition. Furthermore, the  $c$ -axis lattice parameter (14.057 Å) for  $x = 0.87$  is lesser than that (14.319 Å) for  $x = 0.33$  [9]. This modification splits the  $t_{2g}$  and  $e_g$  states of the cobalt 3d orbital. Accordingly, the PDOS of hexagonal  $\text{LiCoO}_2$  (figure 3) reveals that the unoccupied cobalt 3d states show two peaks and that the highest occupied 3d states show three peaks. Strong peaks of the oxygen 2p states are farther from the Fermi level. The net effect is that the charge-transfer bands are shifted to higher energies.

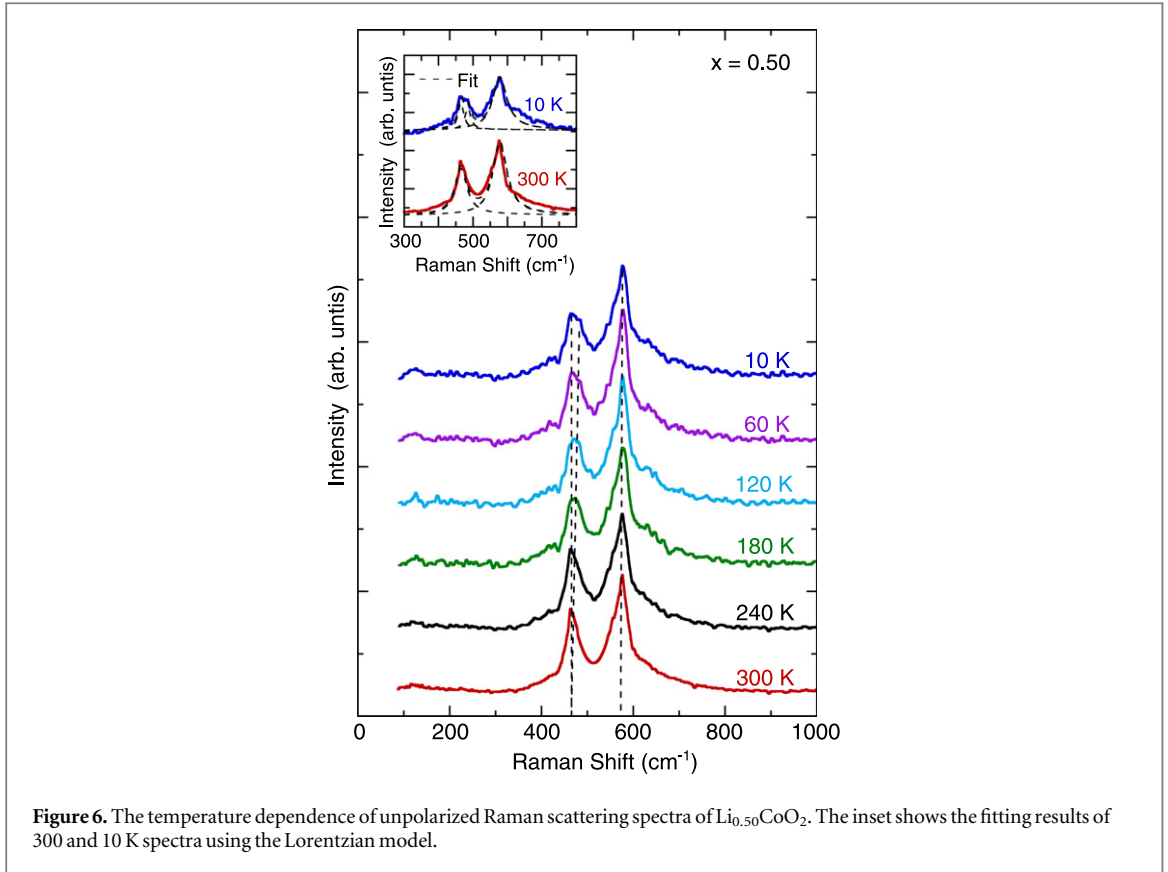
### 3.2. Vibrational properties

Figure 4(a) shows the room-temperature Raman scattering spectra of  $\text{Li}_x\text{CoO}_2$  with six different lithium contents. The spectra comprise two main first-order Raman phonon modes. We fitted these phonon peaks by using a standard Lorentzian profile (the inset of figure 6). The doping dependence of the fitting parameters is shown in figure 5. According to factor group analysis, the pristine sample with  $x = 0.87$  has a hexagonal structure (space group  $R\bar{3}m$ ) containing one formula unit per primitive cell. The  $\Gamma$ -point normal modes can be decomposed as  $A_{1g} + E_g + 2A_{2u} + 2E_{2u}$  [15, 16]. These modes are classified as Raman-active ( $A_{1g} + E_g$ ) and infrared-active ( $A_{2u} + E_{2u}$ ). Thus,  $\text{Li}_{0.87}\text{CoO}_2$  exhibits two strong Raman phonon modes at approximately 489 and 598  $\text{cm}^{-1}$ . The inset of figure 4(a) shows Raman scattering spectra of parallel and cross measurements for  $\text{Li}_{0.87}\text{CoO}_2$ . The 598  $\text{cm}^{-1}$  mode in cross geometry is much more suppressed than the other mode, indicating that it is of  $A_{1g}$  character. By contrast, the 489  $\text{cm}^{-1}$  mode shows  $E_g$  symmetry. The  $E_g$  mode involves in-plane O-Co-O bending motions, whereas the  $A_{1g}$  mode results from out-of-plane Co-O stretching motions [15–18]. The low-intensity broad contributions of phonon modes around 1000 and 1175  $\text{cm}^{-1}$  should be ascribed to multiphonon processes. Notably, spatial maps of the Raman frequency for the  $E_g$  mode (figure 4(c)) show uniform color contrast in each  $\text{Li}_{0.87}\text{CoO}_2$  domain (figure 4(b)), confirming that the frequency of the  $E_g$  mode varies only slightly with location within a sample. This evidence indicates that our  $\text{Li}_{0.87}\text{CoO}_2$  single crystal is in a purely hexagonal phase. This result differs from previous results indicating two coexisting hexagonal phases on the basis of observations of powder forms [16].

Upon a decrease in the lithium content, the positions of the  $E_g$  and  $A_{1g}$  mode shift toward lower frequencies and their linewidths broaden substantially. As indicated by the crystal structure analysis [5–7, 9],  $\text{Li}_x\text{CoO}_2$  samples of  $x = 0.33, 0.43, 0.53,$  and  $0.72$  have the rhombohedral space group and the phase with  $x = 0.50$  belongs to the monoclinic system. Therefore, the frequency of the  $E_g$  mode observed for  $x = 0.87$  (figure 5(a)) differs considerably from that for other doping levels. Furthermore, when lithium was deintercalated, the increase in the  $c$ -axis lattice constant resulted in red-shifting of the frequency of the  $A_{1g}$  mode (figure 5(b)). Our results are in reasonable agreement with recent first-principles calculations of phonon properties of  $\text{LiCoO}_2$  and its delithiated state [30]. The broadening of the  $E_g$  and  $A_{1g}$  modes in compounds with low lithium doping could have been caused by an increase in the lattice disorder.



The temperature-dependent Raman scattering spectra of sample with  $x = 0.50$  are presented in figure 6. The sample with  $x = 0.53$  yielded qualitatively similar results. With a decrease in the temperature, the peak positions of the  $E_g$  and  $A_{1g}$  modes shifted to higher frequencies and the resonance linewidth narrowed. However, the positions of the two modes show peculiar behavior below 200 K. Figure 7 further illustrates the frequency, damping, and oscillator strength of the two modes as a function of temperature. First consider the  $E_g$  mode at approximately  $464 \text{ cm}^{-1}$  in figure 7(a); the phonon mode is associated with in-plane O-Co-O bending vibrations. As the temperature was lowered from 300 to 200 K, the phonon frequency of the  $E_g$  mode increased slightly, as expected for an anharmonic solid. Notably, splitting of the frequencies can be clearly observed below 200 K. The overall amount of splitting is approximately  $18 \text{ cm}^{-1}$  at 10 K. In figure 7(a), the damping is constant



**Figure 6.** The temperature dependence of unpolarized Raman scattering spectra of  $\text{Li}_{0.50}\text{CoO}_2$ . The inset shows the fitting results of 300 and 10 K spectra using the Lorentzian model.

between 300 and 200 K, but decreases below 200 K. The oscillator strength decreases from 300 to 200 K, but exhibits little temperature dependence at lower temperatures.

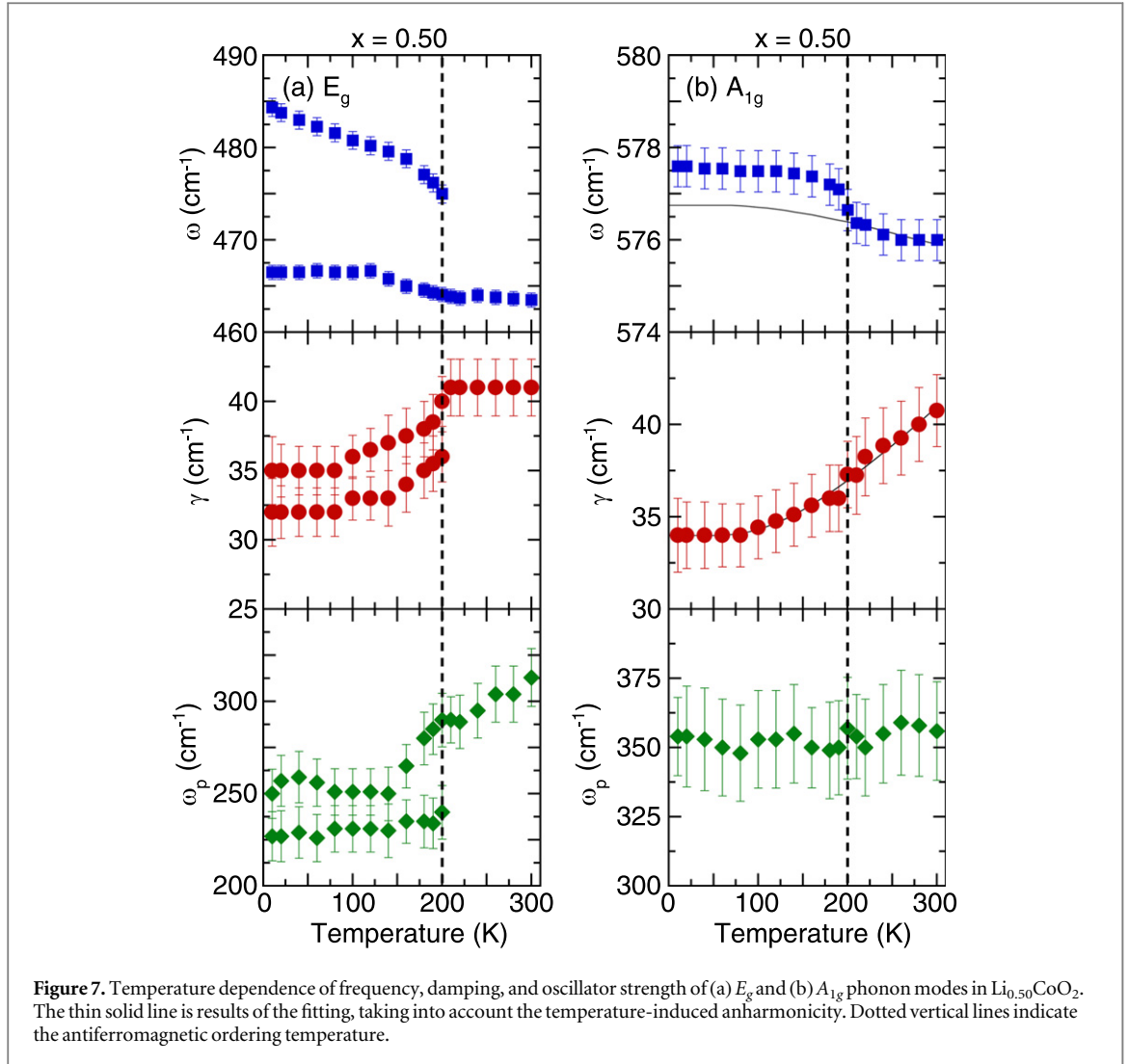
The most striking feature in figure 7(a) is the splitting of the  $E_g$  mode below 200 K, and at 10 K the amplitude of this splitting, which is approximately 4% of the mode frequency, is anomalously large. Since chain-type antiferromagnetic ordering has previously been detected in  $\text{Li}_{0.50}\text{CoO}_2$  at approximately 200 K on the basis of magnetic susceptibility measurements [9], the observed large splitting of the  $E_g$  mode across the phase transition temperature should be closely related to the coupling between the lattice and spin degrees of freedom. Such phonon splitting behavior near  $T_N$  is similar to that of infrared-active phonon modes observed in antiferromagnetic transition metal oxides [26, 31, 32]. We speculate that the doubly degenerate in-plane  $E_g$  phonons are lifted because of strong spin-phonon interaction. Strong magnetoelastic coupling reflects the modulation of the Co-O-Co superexchange interaction by the  $E_g$  phonon in the antiferromagnetic phase and contributes to the anomalous behavior of this mode for  $T < T_N$ . Low-temperature high-resolution synchrotron x-ray diffraction experiments currently under way could facilitate acquiring conclusive evidence for magnetic-order-induced local symmetry breaking in  $\text{Li}_{0.50}\text{CoO}_2$ .

Finally, the temperature dependence of the  $A_{1g}$  mode at approximately  $576 \text{ cm}^{-1}$  is of particular interest (figure 7(b)). This phonon, related to out-of-plane Co-O stretching vibrations, gradually hardens as the temperature decreases from 300 to 200 K. However, the frequency of the  $A_{1g}$  mode changes discontinuously at  $T_N$ ; for  $T < T_N$  the position of the mode continues to increase. In a normal anharmonic solid, with a decrease in the temperature, the phonon frequency should increase, while damping decreases. Anharmonic interactions are relevant to the high-order terms of atomic vibrations, beyond the traditional harmonic terms. The temperature-dependent phonon frequency and linewidth can be written as [33]

$$\omega(T) = \omega_0 + A \left( 1 + \frac{2}{\exp(\hbar\omega_0/2k_B T) - 1} \right), \quad (1)$$

and

$$\gamma(T) = \gamma_0 + B \left( 1 + \frac{2}{\exp(\hbar\omega_0/2k_B T) - 1} \right), \quad (2)$$



where  $\omega_0$  and  $\gamma_0$  are the intrinsic frequency of the optical phonon mode and linewidth broadening because of defects. Parameters  $A$  and  $B$  are the anharmonic coefficients, and  $\frac{1}{\exp(\hbar\omega_0/2k_B T) - 1}$  corresponds to the thermal population factor of acoustic modes. For the analysis of anharmonic contributions to the  $A_{1g}$  mode, the values of  $\omega_0$  ( $\approx 577 \text{ cm}^{-1}$ ),  $\gamma_0$  ( $\approx 34 \text{ cm}^{-1}$ ),  $A$  ( $\approx -1.3$ ), and  $B$  ( $\approx 9.1$ ) were determined. The parameter  $A$  is negative, indicating that the peak shifts to a lower frequency with an increase in the temperature because of anharmonic phonon decay. By contrast, the parameter  $B$  is positive, reflecting linewidth narrowing with a decrease in the temperature. The solid lines in figure 7(b) are theoretical predictions based on equations (1) and (2), and they are in good agreement with the experimental data. Notably, the frequency of the  $A_{1g}$  mode deviates from the theoretical predictions below 200 K. We attribute this deviation mainly to spin-phonon coupling in the antiferromagnetic state of  $\text{Li}_{0.50}\text{CoO}_2$ .

#### 4. Summary

We employed both spectroscopic ellipsometry and Raman scattering spectroscopy to investigate the doping dependence of electronic structure and lattice dynamics in  $\text{Li}_x\text{CoO}_2$  single crystals. Furthermore, we characterized the optical transitions comprehensively by comparing experimental data and the results of first-principles calculations. The optical absorption spectra for  $x$  values in the range of 0.33–0.72 exhibit three features at approximately 1.60, 3.35, and 5.20 eV. The first peak was attributed to a transition between the occupied  $t_{2g}$  to the empty  $e_g$  states of cobalt  $3d$  orbitals. The other two peaks were attributed to charge transfer transitions between oxygen  $2p$  and cobalt  $3d$  states. For the  $x$  value of 0.87, because of the symmetry-breaking-induced distortions of the hybridized Co-O orbitals with shifted oxygen  $2p$  states, its charge-transfer excitations are blue-shifted. Moreover, characteristic changes were observed in the Raman phonon modes of  $E_g$  and  $A_{1g}$  symmetry with a change in the lithium concentration, and the changes were correlated with the crystal structure.

A decrease in the temperature leads to the  $E_g$  phonon mode splitting, and the frequency of the  $A_{1g}$  vibration changes discontinuously at 200 K, which is the antiferromagnetic transition temperature of  $\text{Li}_{0.50}\text{CoO}_2$ . These results suggest that the onset of antiferromagnetic ordering alters the character of atomic displacements, evidencing that strong spin–phonon coupling occurs in  $\text{Li}_{0.50}\text{CoO}_2$ .

## Acknowledgments

HLL thanks technical support for the use of the laser Raman microscope (Raman-11) from Nanophoton Inc. HLL acknowledges financial support from the Ministry of Science and Technology of Republic of China under grant No. NSC 102-2112-M-003-002-MY3.

## References

- [1] Goodenough J B and Kim Y 2010 *Chem. Mater.* **22** 587
- [2] Goldner R B, Chapman R L, Foley G, Goldner E L, Haas T, Norton P, Seward G and Wong K K 1986 *Sol. Energy Mater.* **14** 195
- [3] Mukai K *et al* 2007 *Phys. Rev. Lett.* **99** 087061
- [4] Takahashi Y, Kijima N, Tokiwa K, Watanabe T and Akimoto J 2007 *J. Phys.: Condens. Matter.* **19** 436202
- [5] Hertz J T, Huang Q, McQueen T, Klimczuk T, Bos J W G, Vuciu L and Cava R J 2008 *Phys. Rev. B* **77** 075119
- [6] Motohashi T, Ono T, Sugimoto Y, Masubuchi Y, Kikkawa S, Kanno R, Karppinen M and Yamauchi H 2009 *Phys. Rev. B* **80** 165114
- [7] Miyoshi K, Iwai C, Kondo H, Miura M, Nishigori S and Takeuchi J 2010 *Phys. Rev. B* **82** 075113
- [8] Motohashi T, Sugimoto Y, Masubuchi Y, Sasagawa T, Koshibae W, Tohyama T, Yamauchi H and Kikkawa S 2011 *Phys. Rev. B* **83** 195128
- [9] Ou-Yang T Y, Huang F-T, Shu G J, Lee W L, Chu M-W, Liu H L and Chou F C 2012 *Phys. Rev. B* **85** 035120
- [10] Amatucci G G, Tarascon J M and Klein L C 1996 *J. Electrochem. Soc.* **143** 1114
- [11] van Elp J, Wieland J L, Eskes H, Kuiper P, Sawatzky G A, de Groot F M F and Turner T S 1991 *Phys. Rev. B* **44** 6090
- [12] Czyżyk M T, Portze R and Sawatzky G A 1992 *Phys. Rev. B* **46** 3729
- [13] Ménétrier M, Saadouni I, Levasseur S and Delmas C 1999 *J. Mater. Chem.* **9** 1135
- [14] Kellerman D G, Galakhov V R, Semenova A S, Blinovsky Ya N and Leonidova O N 2006 *Phys. Solid State* **48** 548
- [15] Huang W and Frech R 1996 *Solid State Ion.* **86-88** 395
- [16] Inaba M, Iriyama Y, Ogumi Z, Todzuka Y and Tasaka A 1997 *J. Raman Spectrosc.* **28** 613
- [17] Julien C 2003 *Solid State Ion.* **157** 57
- [18] Wang X, Loa L, Kunc K, Syassen K and Amboage M 2005 *Phys. Rev. B* **72** 224102
- [19] Perdew J P and Wang Y 1992 *Phys. Rev. B* **45** 13244
- [20] Kresse G and Hafner J 1993 *Phys. Rev. B* **48** 13115
- [21] Liechtenstein A I, Anisimov V I and Zaanen J 1995 *Phys. Rev. B* **52** R5467
- [22] Kresse G and Joubert J 1999 *Phys. Rev. B* **59** 1758
- [23] Nekrasov I A, Streltsov S V, Korotin M A and Anisimov V I 2003 *Phys. Rev. B* **68** 235113
- [24] Lee J S, Lee Y S, Noh T W, Char K, Park J, Oh S-J, Park J-H, Eom C B, Takeda T and Kanno R 2001 *Phys. Rev. B* **64** 245107
- [25] Zhou J, Zheng P and Wang N L 2008 *J. Phys. Condens. Matter.* **20** 055222
- [26] Hsu H C, Chou F C, Koyama K, Watanabe K and Liu H L 2009 *Phys. Rev. B* **79** 155109
- [27] Johannes M D, Mazin I I and Singh D J 2005 *Phys. Rev. B* **71** 205103
- [28] Wang N L, Zheng P, Wu D, Ma Y C, Xiang T, Jin R Y and Mandrus D 2004 *Phys. Rev. Lett.* **93** 237007
- [29] Hwang J, Yang J, Timusk T and Chou F C 2005 *Phys. Rev. B* **72** 024549
- [30] Gong X *et al* 2013 *Int. J. Electrochem. Sci.* **8** 10549
- [31] Massidda S, Posternak M, Baldereschi A and Resta R 1999 *Phys. Rev. Lett.* **82** 430
- [32] Luo W, Zhang P and Cohen M L 2007 *Solid State Commun.* **142** 504
- [33] Menendez J and Cardona M 1984 *Phys. Rev. B* **29** 2051 and references therein